A numerical study on regularization and key rheological parameters in the evolution of rigid zones in Herschel-Bulkley fluids

M. Elalem[a], F. Messelmi[b], H. Taibi[c], A. Rabehi[d], A. Douara[e], and M, Benghanem[f,*]

[a]*Ziane Achour University of Djelfa, Faculty of Exact Sciences and Computer Science, Department of Physics, Laboratory of Development in Physiochemistry of Materials and Environment, Algeria.*
[b]*Ziane Achour University of Djelfa, Faculty of Exact Sciences and Computer Science, Department of Mathematics, Djelfa 17000, Algeria.*
[c]*Ziane Achour University of Djelfa, Faculty of Technology Science, Department of Mechanical Engineering, Algeria.*
[d] *Laboratory of Telecommunication and Smart Systems (LTSS), Faculty of Science and Technology, University of Djelfa, PO Box 3117, Djelfa 17000 Algeria.*
[e]*Faculty of Science and Technology, Tissemsilt University, Tissemsilt, 38000, Algeria.*
[f]*Physics Department, Faculty of Science, Islamic University of Madinah, Madinah, 42351, Saudi Arabia.*
[*]*e-mail: mbenghanem@iu.edu.sa*

Received 23 May 2025; accepted 18 August 2025

Regulating the formation of rigid zones in viscoplastic fluids is essential for accurate numerical modeling and practical applications. This paper presents a numerical study on the control and minimization of rigid zones in Herschel-Bulkley fluids during flow at the yield stress threshold within a confined square domain. The Papanastasiou regularization method is employed to ensure a smooth transition between fluid and rigid-like zones. This study systematically analyzes the influence of key rheological parameters and the regularization approach on the suppression and reduction of these zones. The influence of the regularization parameter m on rigid zone formation during flow is investigated, along with the effect of the critical shear rate for different values of this parameter. Additionally, the impact of inlet pressure on the rigid zone area is examined, followed by an in-depth analysis of its effect for various critical shear rate values to explore their combined influence. Furthermore, the study explores the influence of the consistency factor and the power-law index on rigid zones during flow. The findings highlight optimal parameter selection strategies to suppress or minimize rigid zones at the yield stress threshold, ensuring improved numerical accuracy in viscoplastic fluid simulations.

Keywords: Papanastasiou regularization parameter; critical shear rate; rigid zones; Herschel-Bulkley fluid; unsteady flow; consistency factor; pressure; power-law index.

DOI: https://doi.org/10.31349/RevMexFis.72.011702

1. Introduction

Non-Newtonian fluids play a pivotal role across diverse natural phenomena and industrial processes. Their unique rheological behavior is critical in applications ranging from geophysical flows (*e.g.*, mudslides and volcanic lava) to manufacturing sectors including food production, pharmaceutical development, construction materials (like concrete and ceramics), and coating technologies (inks, paints, and polymer solutions) [1, 2]. A defining feature of these fluids is their yield stress, which serves as a key parameter in rheological modeling frameworks such as the Herschel-Bulkley formulation.

The Herschel-Bulkley model has become a cornerstone for characterizing viscoplastic fluids due to its nonlinear constitutive aligns. This has spurred extensive research into both theoretical analysis and computational modeling of such flows. Notable contributions include Huilgol et al. [3], who developed an innovative pipe flow analysis using extended Lagrangian methods. Concurrently, Vajravelu *et al*. [4] examined hemodynamic applications, quantifying how pressure gradients, yield stress, and vessel elasticity influence blood flow dynamics when modeled as a Herschel-Bulkley fluid. Complementing these studies, Saramito [5] made substantial advances in numerical simulation techniques, identifying key computational obstacles and accuracy limitations in yield stress fluid modeling.

Herschel-Bulkley fluids exhibit a distinct transition in their behavior. Below the yield stress threshold, they act as rigid bodies. Once the applied stress exceeds this threshold, they transition into a flowing state, behaving like a fluid [6]. However, numerical simulations of such fluids present significant challenges due to their complex rheological properties, particularly the discontinuity in their constitutive laws. To overcome these challenges, various regularization techniques have been developed. Among them, the widely used Papanastasiou model [7] introduces an exponential smoothing function to enhance numerical stability. Alternative approaches, such as the Bercovier and Engelman regularization [8] and viscous regularization [9], have also been employed to address the singularity at the yield stress threshold, thereby improving computational accuracy. Additionally, the models introduced in [10, 11] were specifically designed to

resolve this singularity in viscoplastic fluids. Their effectiveness has been assessed by comparing their results with those obtained from previously established regularization methods.

Herschel-Bulkley fluids consist of dispersed particles within a solvent. At low concentrations, these particles primarily contribute to an increase in viscosity. However, as their concentration rises, interactions and collisions between particles intensify, leading to a pasty consistency and the emergence of rigid zones. Several studies have explored the formation and distribution of these rigid zones to assess the impact of various parameters. For instance, Hassan *et al*. [12] analyzed Rayleigh-Bénard convection in such fluids and demonstrated how Rayleigh number influences the expansion of flowing and non-flowing zones in confined domains. Recent investigations [13, 14] have systematically evaluated how dimensionless parameters including the Reynolds number, Oldroyd number, power-law index, and Papanastasiou regularization coefficient affect the formation and positioning of stagnant zones in yield stress fluids. The choice of the Papanastasiou parameter m remains particularly contentious, as this value critically governs yield surface continuity. A comparative analysis by Syrakos *et al*. [15] revealed nearly indistinguishable yield surfaces for $m = 1000$ and =10000, though the former produced smoother interfacial transitions, prompting its widespread preference. This aligns with broader observations [16–20] documenting jagged, irregular yield lines when excessively high m values are employed.

Notably, $m = 1000$ has emerged as a de facto standard in many studies [15, 19, 21], yet substantial discrepancies persist. For example, Jeong [22] implemented an unusually low = 0.3, whereas Patel *et al.* [23] adopted an extreme value of $m = 10^7$, underscoring the ongoing difficulty in establishing a universally optimal parameter that reconciles computational efficiency with phenomenological precision.

Equally critical is the determination of the threshold shear rate γ_c, which dictates the identification of rigid zones. Reported values exhibit remarkable variability: Lin *et al*. [24] identified $\gamma = 0.01$ s^{-1} for kaolinite suspensions (at PH=5 across varying concentrations), while Mossaz *et al*. [25] employed a significantly lower $\gamma = 0.0001$ s^{-1} for polymer gel systems.

This study seeks to examine the suppression and minimization of rigid zones during the flow of a Herschel-Bulkley fluid at the yield stress threshold. It focuses on analyzing how rheological parameters and the regularization approach influence the formation and reduction of rigid zones during flow. Special attention is given to the role of Papanastasiou's regularization parameter, the critical shear rate, and inlet pressure in controlling these zones. Additionally, the study examines the impact of the consistency factor and power-law index on the extent of rigid zones, providing insight into optimal parameter selection to mitigate their formation and ensure improved numerical accuracy in viscoplastic fluid simulations.

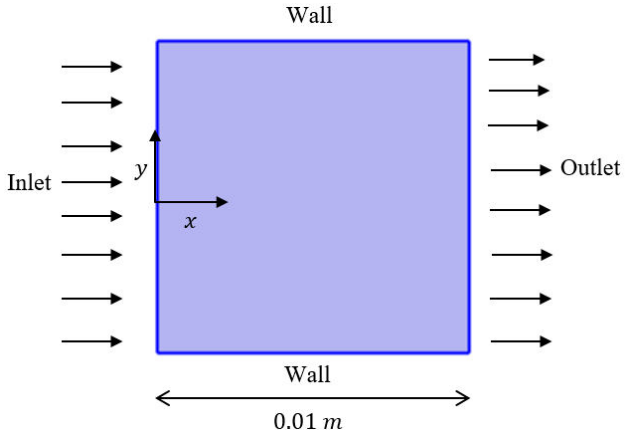

FIGURE 1. Domain of flow.

TABLE I. Rheological characteristics of the used concrete [26].

Material	ρ (kg/m^3)	τ_y (Pa)	k (Pa · s^n)	n
Concrete	1370	5	2.42	0.552

2. Problem description

In this numerical study, the flow of fresh concrete, modeled as a Herschel-Bulkley fluid, is analyzed within a two-dimensional confined square domain. This simulation is conducted in an unsteady state. Figure 1 illustrates the computational setup, where the square domain has a side length of 0.01 m. The flow is driven by an imposed inlet pressure of $p = 20$ Pa, while the initial velocity is set to $u_{\text{ini}} = 0.001$ m/s. A no-slip condition is enforced on all walls. The rheological properties of fresh concrete are summarized in Table I, assuming the material is incompressible and follows an isothermal, laminar flow regime.

3. Mathematical formulation

The governing aligns for fluid flow are the continuity align and the momentum align, respectively, as follows:

$$\nabla \cdot U = 0, \tag{1}$$

$$\rho \frac{\partial U}{\partial t} + \rho (U \cdot \nabla) U = \nabla \left[-pI + \tau \right] + f. \tag{2}$$

In the study of viscoplastic fluids, the Herschel-Bulkley model is widely used to describe shear stress τ with a yield stress threshold τ_y. The constitutive align is expressed as follows [27]:

$$\tau = \begin{cases} \left(k|\gamma|^{n-1} + \dfrac{\tau_y}{|\gamma|} \right) \gamma, & \text{if} \quad |\tau| > \tau_y, \\ |\gamma| = 0, & \text{if} \quad |\tau| \leq \tau_y. \end{cases} \tag{3}$$

In the Herschel-Bulkley viscoplastic model, the fluid exhibits two distinct behaviors depending on the applied stress. If the stress surpasses the yield limit, the fluid transitions into

a flowing state, displaying pseudo-plastic behavior. Conversely, when the stress remains below the yield threshold, the fluid does not flow and instead behaves as a rigid body, with its viscosity tending to infinity, *i.e.* $\lim_{\gamma \to 0} \mu(\gamma) = \infty$ [28, 29]. In this state, the material behaves as a rigid body with zero deformation. Mathematically, these rigid domains are characterized by null shear rate values, as specified in the following relation [30]:

$$\Omega_r = \{\, x \in \Omega, \geq 0 : \ |\gamma(U(x,y))| = 0 \,\}. \tag{4}$$

In the Herschel-Bulkley formulation, a computational singularity arises when the shear rate diminishes to zero, posing a challenge for numerical simulations. To overcome this, several regularization techniques have been proposed in the literature [31–33]. Among these approaches, the Papanastasiou regularization method is employed to ensure a smooth transition between the rigid and fluid-like states. This method modifies the stress expression by introducing a regularization parameter m, leading to the following formulation [34]:

$$\tau = k|\gamma|^{n-1} + \left(\frac{\tau_y}{|\gamma|}\right)\left[1 - e^{-m|\gamma|}\right]\gamma, \tag{5}$$

and the viscosity takes the formula:

$$\mu(\gamma) \ = \ k|\gamma|^{n-1} + \left(\frac{\tau_y}{|\gamma|}\right)\left[1 - e^{-m|\gamma|}\right]. \tag{6}$$

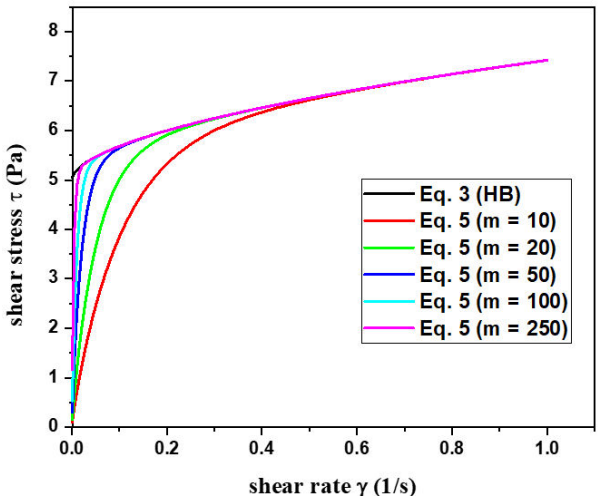

FIGURE 2. Comparison between the original Herschel-Bulkley model Eq. (3) and its regularized version using the Papanastasiou method Eq. (5) for various values of the regularization parameter m.

To illustrate the effect of the regularization parameter m on the constitutive behavior, Fig. 2 presents the shear stress as a function of the shear rate, calculated from Eq. (3) and (5) using the rheological parameters selected in this study. The regularization parameter m is varied over values of 10, 20, 50, 100, and 250.

Figure 2 clearly demonstrates that larger values of m produce a sharper transition from the rigid to the flowing state, closely approaching the original Herschel-Bulkley model as $m \to \infty$. In contrast, smaller values of m result in a smoother transition near zero shear rate, which helps avoid numerical singularities and enhances the stability of simulations.

This conceptual illustration underlines the importance of selecting an appropriate m value in numerical modeling, balancing physical accuracy and computational robustness.

Zones where the shear rate does not exceed the critical shear rate, *i.e.*, $\gamma \leq \gamma_c$, which corresponds to $\tau \leq \tau_y$, can be classified as rigid zones forming during the flow [35]. Mathematically, based on, these zones can be expressed as follows. Since this study deals with unsteady flow, a time-dependent term (t) is incorporated into the formulation:

$$\Omega_r = \left\{\, x \in \Omega, \ t \geq 0 : \ \left|\gamma(U(x,y,t))\right| \leq \gamma_c \,\right\}. \tag{7}$$

In the COMSOL Multiphysics simulation, rigid zones were identified by evaluating the local shear rate field $|\gamma|$ at each time step. A logical condition was applied in the post-processing phase using the `Expression` feature in the `Results` section.

Regions where the shear rate satisfies the condition $|\gamma| \leq \gamma_c$ were extracted and visualized as rigid domains evolving over time.

The Papanastasiou regularization parameter was chosen as $m = 10$. These values were used in the simulations, and their influence on the results will be discussed in later sections.

4. Validation and grid study

To validate the numerical approach, we ensured the accuracy of the steady-state solution, which serves as the initial condition for unsteady flow simulations. This was achieved by comparing the computed velocity domain with the exact analytical solution derived from theoretical calculations. The velocity domain is given by $\mathbf{U} = Vu^*(y)\,\mathbf{e}_x$. The analytical velocity profile is described by the following relations Eq. (8) [36–40].

$$u^*(y) = \frac{1}{M} f^* \times \begin{cases} \left(\frac{y_0}{H}\right)^M - \left(\frac{y_0 - y}{H}\right)^M, & 0 \leq y \leq y_0, \\ \left(\frac{y_0}{H}\right)^M, & y_0 \leq y \leq H - y_0, \\ \left(\frac{y_0}{H}\right)^M - \left(\frac{y - (H - y_0)}{H}\right)^M, & H - y_0 \leq y \leq H, \end{cases} \tag{8}$$

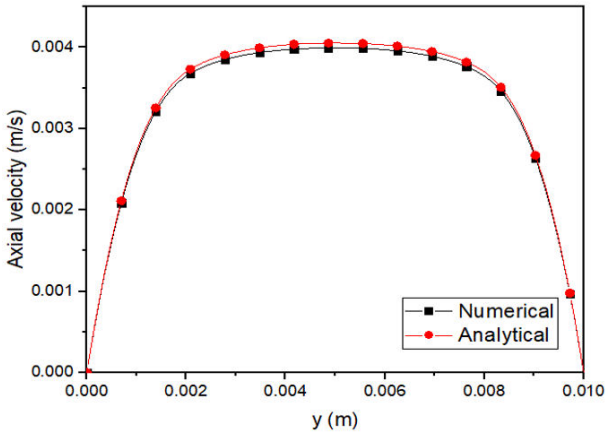

FIGURE 3. Numerical and theoretical comparison of axial velocity profiles.

where,

$$M = 1 + \frac{1}{n}, \quad f^* = \left(\frac{fH}{K}\right)^{\frac{1}{n}} \frac{H}{V}, \quad y_0 = \frac{H}{2} - \frac{\tau_y}{f}.$$

A comparison has been made between the numerical velocity profile produced at $x = H/2$ using COMSOL Multiphysics 6.0 and the theoretical velocity profile derived from the analytical relations. Strong agreement between the analytical and numerical conclusions is revealed by the velocity distributions in Fig. 3, indicating the dependability of the numerical model. Ensuring an accurate steady-state solution is crucial for reliable transient flow simulations, as it prevents numerical instabilities and ensures a physically realistic initial state. Comparing analytical and numerical velocity profiles reinforces confidence in the computational model's accuracy in capturing complex flow behaviors.

Choosing the grid for the numerical simulations carefully is crucial to guaranteeing the correctness of the findings. In this study, a structured mesh was generated, and different grid sizes were tested to determine the appropriate mesh resolution.

Figure 4 displays the axial velocity profiles for four different grid sizes at $t = 0.05$ s, the selected moment when the fluid attains its final stabilized state. The velocity distributions from Grid-3 and Grid-4 exhibit a strong similarity, prompting the choice of Grid-3, which comprises 10,500 elements.

Table II presents the influence of grid resolution on the peak axial velocity at the mid-section of the domain. The relative error between the velocities obtained with the last two grids, Grid-3 and Grid-4, is only 0.41%. Therefore, Grid-3 is adopted for all numerical simulations in this study.

TABLE II. Axial velocity and relative error for different mesh sizes.

Grid number	Number of elements	Maximum velocity (m/s)	Relative Error (%)
Grid-1	1500	0.0038490	1.66
Grid-2	9750	0.0039128	1.80
Grid-3	10500	0.0039834	0.41
Grid-4	34034	0.0039999	–

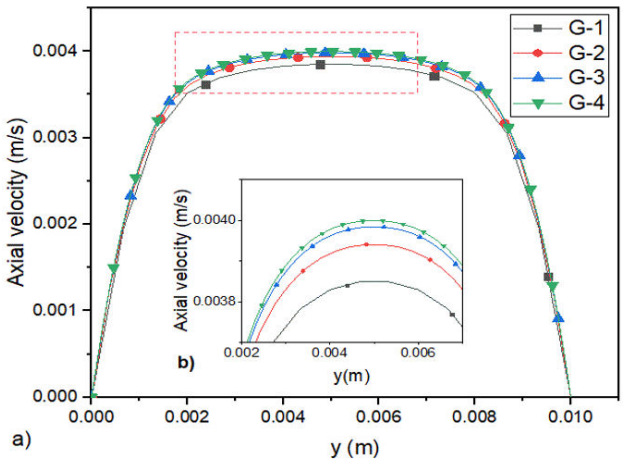

FIGURE 4. Axial velocity profiles along y direction in the centre-line of the cross section for various grid sizes.

5. Results and discussion

5.1. Combined influence of the regularization parameter and critical shear rate on rigid zone formation

The results are presented to highlight the influence of the Papanastasiou regularization parameter m on the formation of rigid zones during flow, at a constant critical shear rate. This study investigates how different values of this parameter affect the development of these zones as the material deforms beyond the yield stress threshold.

Figure 5 illustrates the temporal evolution of the rigid zone area for different values of the Papanastasiou regularization parameter m at a critical shear rate of $\gamma_c = 0.01\,\mathrm{s}^{-1}$. The results show that for lower values of m (*e.g.*, $m = 10\,\mathrm{s}$), the rigid zones remain minimal. However, as m increases

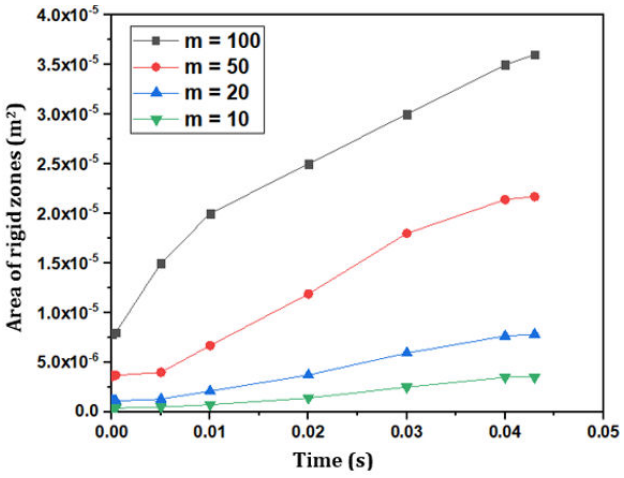

FIGURE 5. Evolution of the rigid zones area over time for various values of the Papanastasiou regularization parameter m.

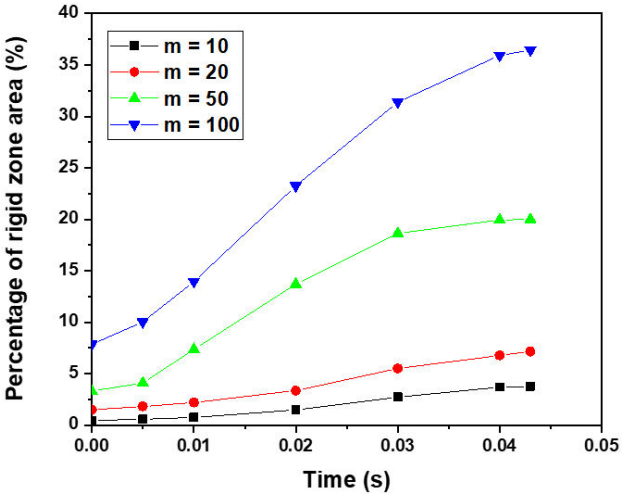

FIGURE 6. Evolution of rigid zone percentage over time for various regularization values m.

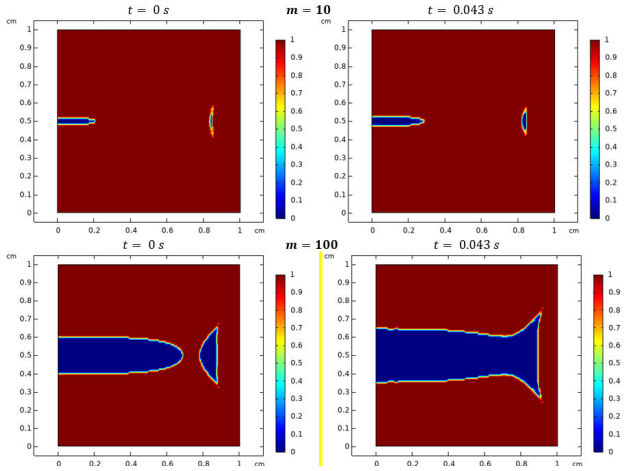

FIGURE 7. Scenario of rigid zone formation for two representative values of the Papanastasiou regularization parameter ($m = 10$ and $m = 100$).

(*e.g.*, 20, 50, and 100 s), these zones expand significantly, with the most pronounced rigid zones observed at $m = 100$ s. This trend indicates that the regularization parameter has a substantial impact on the numerical depiction of rigid zones during flow. Higher values of m prolong the persistence of these zones and increase their extent, which suggests that the regularization influences the model's ability to capture the transition between flowing and non-flowing regions. This expansion may not be purely physical but rather a numerical artifact associated with the way the regularization scheme approximates the transition between yielded and unyielded zones. Consequently, an appropriate selection of m is crucial to ensuring that the predicted rigid zones remain consistent with the expected physical behavior of the fluid.

The increase in the size of rigid zones with higher values of m is due to the numerical effects of this parameter rather than the actual physical behavior of the fluid. In numerical simulations, increasing m makes the transition between fluid and rigid zones more abrupt, leading to an unrealistic representation of rigid zones during flow. This effect arises because large values of m numerically amplify the yield stress effect, artificially increasing the apparent viscosity even after exceeding the critical stress and preventing the rigid zones from disappearing as expected physically. At lower values of m, the transition is smoother, allowing the fluid to flow as expected once the yield stress is exceeded, with minimal or no rigid zones. However, as m increases, rigid zones become more pronounced and persist for longer durations, indicating that the choice of this parameter must be made carefully to avoid misinterpreting numerical results.

Thus, the choice of m directly impacts the numerical predictions of rigid zones, reinforcing the need for careful parameter selection to ensure meaningful and physically accurate simulations.

To complement the absolute area data shown in Fig. 5, the following figure presents the rigid zones as a percentage of the total simulation domain area. This relative measure enhances the understanding of the spatial significance of rigid zones during the flow.

Figure 6 illustrates the evolution of the rigid zones area expressed as a percentage of the total simulation domain area over time for different values of the regularization parameter m. Presenting the data in relative terms provides a clearer understanding of how the rigid zones develop spatially within the entire flow domain during the simulation.

Figure 7 illustrates the progression of rigid zone formation over time for two representative values of the Papanastasiou regularization parameter ($m = 10$ and $m = 100$). These visual representations offer a clear perspective on the growth and stabilization of rigid zones, emphasizing the impact of the regularization parameter on the solidification process.

Expanding on the previous analysis of the Papanastasiou regularization parameter at a fixed critical shear rate, the subsequent analysis explores the combined effects of both m and γ_c on the formation of rigid zones during flow. By systematically varying these two parameters, this part of the study provides deeper insight into their interaction, highlighting how their interplay influences the emergence and extent of rigid zones during the deformation process.

Figure 8 illustrates the temporal evolution of the rigid zone area during flow for various values of the critical shear rate γ_c, analyzed across three different values of the Papanastasiou regularization parameter ($m = 10, 100, 250$). The results demonstrate a clear interactive relationship between m and γ_c in governing the formation and extent of rigid zones during deformation. Specifically, increasing γ_c leads to more pronounced rigid zones, particularly at higher values of m. For instance, when $m = 250$ s, rigid zones persist even at moderate critical shear rates and are only eliminated when γ_c is reduced to $10^{-4}\,\mathrm{s}^{-1}$. In contrast, for $m = 10$ s, the rigid zones become nearly absent already at $\gamma_c = 10^{-3}\,\mathrm{s}^{-1}$.

These results underscore the role of the regularization parameter in controlling the transition rate from rigid-like to fluid-like behavior: higher values of m prolong the rigid zone

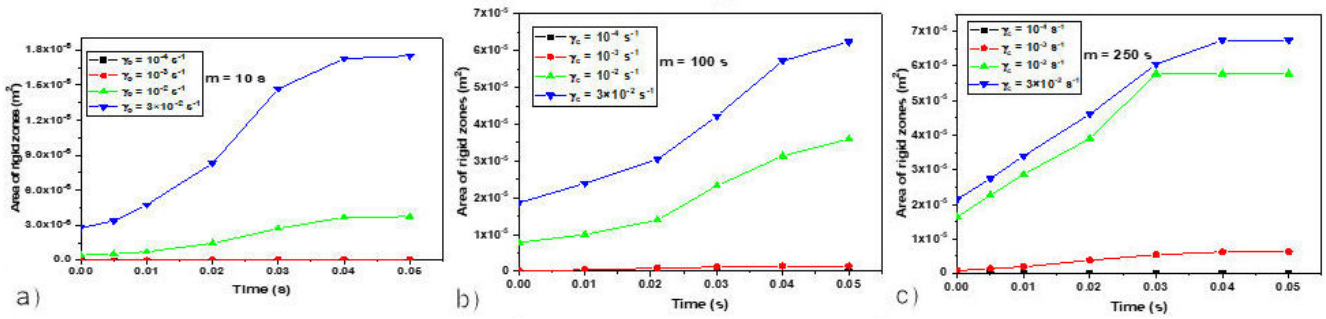

FIGURE 8. Variation of the rigid zone area over time for different critical shear rates and Papanastasiou regularization parameters ($m = 10$, $m = 100$, and $m = 250$).

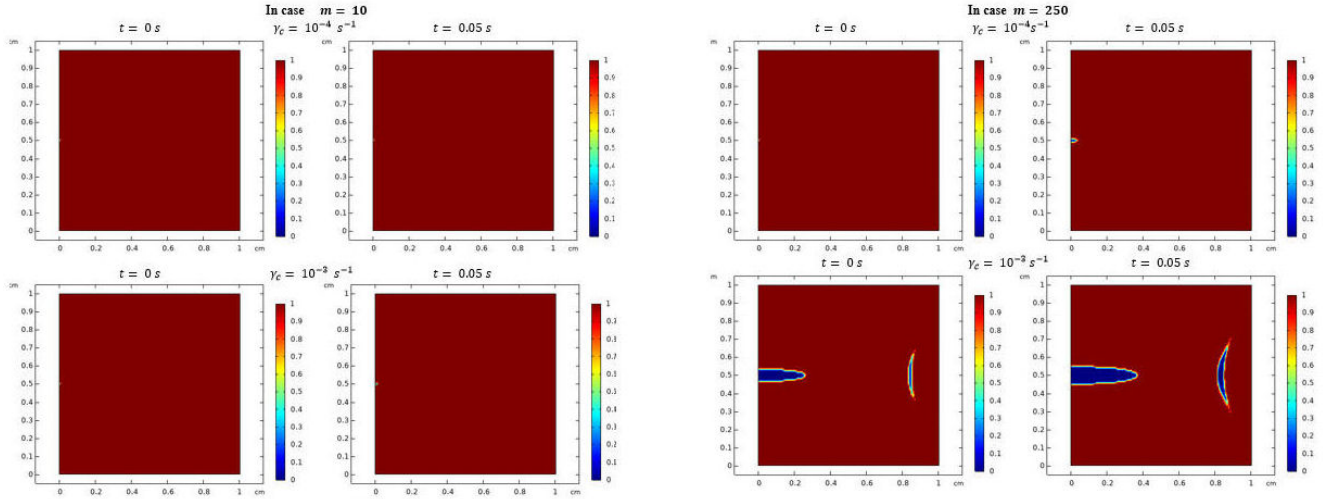

FIGURE 9. Scenario of rigid zone formation for different critical shear rate values at two Papanastasiou regularization parameters ($m = 10$ and 250).

response, necessitating lower values of γ_c to initiate full flow. Additionally, the response to changes in γ_c varies with m, being more gradual at low m, and significantly sharper at high m. This indicates that γ_c cannot be tuned independently, but must be carefully coordinated with the selected m value. From this analysis, a fundamental guideline emerges: when employing high critical shear rates, smaller values of the regularization parameter should be used to avoid artificial solidification during flow. Conversely, for large m, a very low γ_c becomes essential. The findings highlight the importance of a coupled calibration strategy between m and γ_c, ensuring a realistic and physically consistent description of viscoplastic flow without the emergence of nonphysical rigid zones.

Based on the previous analysis, Fig. 9 presents selected snapshots from the simulation to illustrate the evolution of rigid zones over time for different values of the critical shear rate, across two representative cases of the regularization parameter ($m = 10$ and $m = 250$). These results reinforce the understanding of how rheological parameters influence the solidification dynamics and the development of rigid zones during flow.

5.2. Impact of inlet pressure and critical shear rate on rigid zones

In this study, the impact of the applied inlet pressure on the area of rigid zones was analyzed during the flow. A constant critical shear rate of $\gamma_c = 0.001\,\mathrm{s}^{-1}$ and a Papanastasiou regularization parameter of $m = 10\,\mathrm{s}$ were applied. The analysis was conducted at a specific time when the rigid zones reached their stabilized state.

The results, illustrated in Fig. 10, show the impact of inlet pressure on the area of rigid zones during flow. It is observed that increasing the inlet pressure leads to a gradual decrease in the area of rigid zones, a behavior consistent with the expected rheological response of viscoplastic fluids. At lower pressures, despite the material being in a flowing state, rigid zones persist due to locally insufficient shear stress. As the pressure increases, the overall shear stress distribution becomes more uniform and intense, progressively reducing the rigid zones until they become nearly negligible at higher pressures.

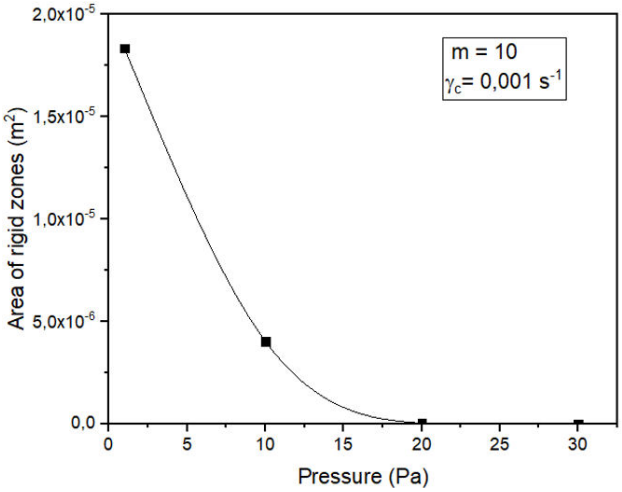

FIGURE 10. Impact of Inlet pressure on the area of rigid zones.

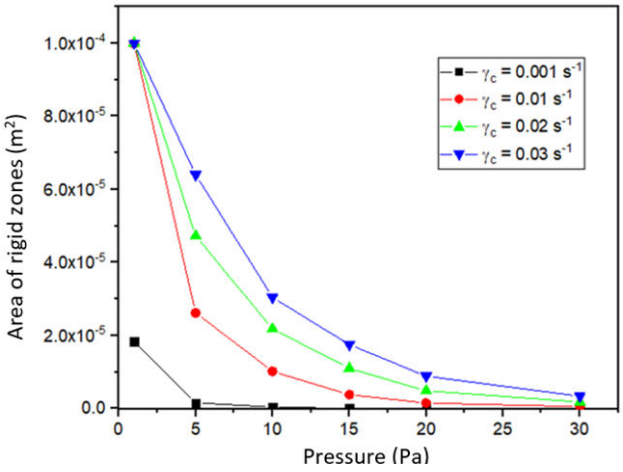

FIGURE 11. Variation of rigid zone area with Inlet pressure at different values of critical shear rates.

Since the study is conducted at the yield stress threshold, the results indicate that pressure variations influence the extent of rigid zones within the flowing material rather than triggering the onset of flow. As the inlet pressure rises, more zones of the fluid experience shear stress values significantly above the yield stress threshold, leading to a more homogeneous deformation field. At sufficiently high pressures, the influence of the yield stress diminishes, and the material behaves increasingly like a power-law fluid, where the contribution of the yield stress to the overall resistance becomes negligible. Furthermore, the findings confirm an inverse relationship between inlet pressure and the area of rigid zones, emphasizing that even within the flowing regime, pressure variations play a key role in modifying the rigid like structures embedded in the viscoplastic material. This underscores the importance of controlling inlet pressure in industrial applications to manage the spatial distribution of rigid zones and ensure stable and efficient flow.

After analyzing the impact of the applied inlet pressure on the rigid zones area at a fixed critical shear rate, an additional study was conducted to explore how this area changes when the critical shear rate is adjusted in each simulation, considering the impact of pressure. This analysis aims to understand the interplay between these two parameters and determine the optimal conditions to minimize rigid zones during flow.

Figure 11 depicts the variation of the rigid zone area as a function of the applied pressure for different critical shear rate values. The results show that choosing a low critical shear rate, such as $\gamma_c = 10^{-3}\,\mathrm{s}^{-1}$, contributes to a reduction in the rigid zone area during flow, particularly when combined with sufficient applied pressure, which aligns with the expected physical behavior of the material. However, it is observed that at low pressure, even with a small critical shear rate, the rigid zone area remains larger, while increasing the pressure reduces this area, yielding results more consistent with the material's physical reality.

These results can be explained by relying on the dynamic balance between the critical shear rate and the applied pressure in the regularized Herschel-Bulkley model. A small critical shear rate makes the material more sensitive to deformation, reducing rigid zone formation. However, at low pressure, this deformation may not be sufficient to fully break down the rigid structure, leading to larger rigid zones than anticipated. Conversely, when choosing a higher critical shear rate, its influence on rigid zone evolution becomes more pronounced, requiring higher pressure to ensure sufficient deformation and reduce rigid zones. Therefore, the results indicate that increasing the critical shear rate must be accompanied by raising the applied pressure to achieve results that more accurately reflect the material's physical behavior during flow.

These findings highlight the importance of balancing the critical shear rate and the applied pressure to achieve realistic and accurate simulations of viscoplastic material flow. Selecting a small critical shear rate is a suitable choice to minimize rigid zones, but it requires higher pressure to ensure their disappearance or significant reduction. Conversely, when opting for higher critical shear rate values, the applied pressure must be increased even further to prevent the persistence of undesired rigid zones. This approach improves simulation accuracy and enhances the reliability of the results in engineering and industrial applications.

5.3. Influence of consistency factor and power-law index on the area of rigid zones

Numerical simulations were conducted to examine the evolution of rigid zones during flow. by independently varying the consistency factor and the power-law index while keeping the other rheological properties constant. This approach provides a clearer understanding of how each parameter individually affects the evolution of rigid zones during flow.

Initially, the influence of the consistency factor on rigid zones over time was examined. As shown in Fig. 12, the area of rigid zones increases significantly with higher values of the consistency factor k. For high k values (*e.g.*, $k = 150\,\mathrm{Pa}\cdot\mathrm{s}^n$), the material exhibits a greater tendency to solidify, and the

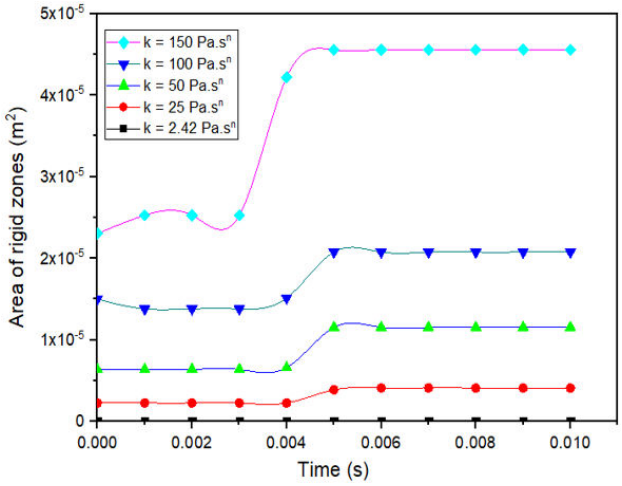

FIGURE 12. Evolution of the rigid zones area over time for various values of the effect consistency factor.

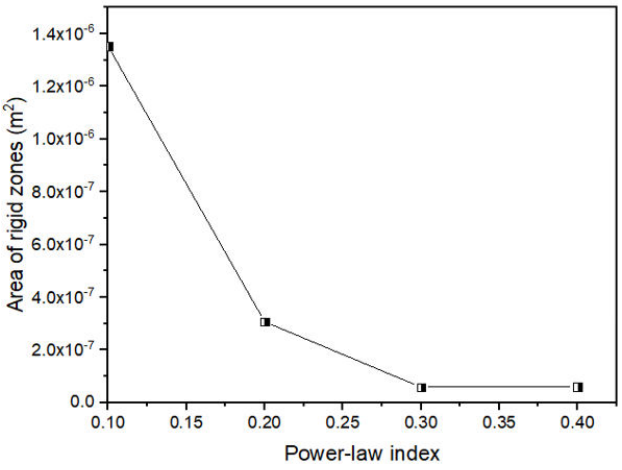

FIGURE 13. Effect of the power-law index on the area of rigid zones.

rigid zone area expands markedly, reaching a steady state after a short period. In contrast, for low consistency factor values (*e.g.*, $k = 2.42\,\text{Pa}\cdot\text{s}^n$), the material becomes more fluid, reducing the size of the rigid zones and slowing their formation.

On the other hand, Fig. 13 illustrates the influence of the power-law index on the rigid zone area. The curve shows a sharp decline in the rigid zone area as the power-law index (n) increases from 0.1 to 0.4. This behavior is attributed to the fact that increasing n reduces the material's viscosity in low strain rate regions, decreasing its tendency to solidify, and consequently shrinking or nearly eliminating the rigid zones.

Integrating these findings highlights a complex inverse correlation between the consistency factor and the power-law index in governing the formation of rigid zones. While increasing the consistency factor promotes rigid zone formation, this effect can be counterbalanced if accompanied by an increase in the power-law index, mitigating the influence

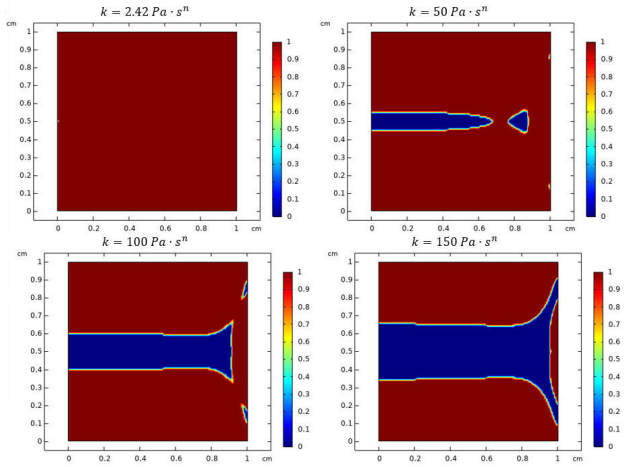

FIGURE 14. Visualization of rigid zones under varying consistency factors.

of the consistency factor. This interaction suggests the existence of a rheological equilibrium point where precise control of rigid zone size is possible, opening avenues for optimizing concrete mix designs to reduce unwanted solidification.

This analysis highlights that studying both parameters together provides a deeper understanding of material evolution during flow, which is crucial in applications such as fresh concrete pumping. Adjusting rheological properties can ensure material stability and prevent early solidification or blockages in pipes and molds.

Thus, exploring the coupled effects of k and n not only enhances the understanding of non-Newtonian flow regimes but also opens pathways for optimizing material formulations to achieve desired flow behaviors, ultimately bridging the gap between theoretical rheology and practical engineering applications.

To further illustrate these results, Fig. 14 presents visual snapshots of the rigid zones for four distinct consistency factor values at the final stage of flow. These images reveal the distribution of rigid zones, emphasizing how higher consistency factors lead to larger and more stable rigid zones, while lower factors limit rigid zone formation. Such visual representations reinforce the numerical findings and provide an intuitive understanding of the material's behavior under varying rheological conditions.

6. Conclusion

In this numerical study, the flow of fresh concrete, modeled as a Herschel-Bulkley fluid, is analyzed within a two-dimensional confined square domain. This simulation is conducted in an unsteady state. The study began with a validation step, where the numerically computed horizontal velocity profile in steady-state conditions was compared against an analytical velocity distribution derived from theoretical formulations. This comparison allowed for an assessment of numerical accuracy. Following this, the study then explored how the regularization parameter m influences the formation

of rigid zones. Additionally, the effect of the critical shear rate on shaping these zones was examined under different values of m (10, 100 and 250). The findings indicated that increasing either parameter results in an enlargement of rigid zones. To achieve reliable numerical outcomes, a low critical shear rate should be paired with a high regularization parameter, or vice versa, to maintain flow stability and prevent artificial solidification. Further analysis was conducted to assess the effect of inlet pressure on rigid zones. The results indicate that as the inlet pressure increases, the fluid exhibits a transition towards a behavior resembling that of a power-law fluid. This suggests that under high-pressure conditions, the apparent viscosity decreases, leading to a response closer to that of a generalized Newtonian fluid. This effect was further examined by varying the critical shear rate, showing that higher values of the critical shear rate necessitate an increase in inlet pressure to ensure numerical consistency in capturing the fluid's physical behavior. Finally, the influence of the consistency factor K and the power-law index n on the rigid zones were analyzed. The study revealed that an increase in K enhances the formation of rigid zones during flow, whereas a higher n reduces them. This highlights a rheological balance that could be leveraged to optimize material design and mitigate undesirable solidification.

TABLE I. Nomenclature

A	Area of the rigid zones (m^2)
p	Pressure (Pa)
I	Unit tensor (1)
f	External body forces (N/m^3)
∇U	Velocity gradient (s^{-1})
$(\nabla U)^T$	Transpose (s^{-1})
Ω	Flow domain (1)
Ω_r	Rigid zones (1)
M, y_0	Constants of theoretical velocity (1)
u^*	Non-dimensional velocity (1)
f^*	Non-dimensional gradient force (1)
γ	Shear rate (s^{-1})
γ_c	Critical shear rate (s^{-1})
μ	Viscosity (Pa·s)
t	Time of flow (s)
m	Papanastasiou regularization parameter (s)
H	Dimension of domain (m)
(x, y)	Point coordinates (1)
V	Reference velocity (m/s)
ρ	Density (kg/m^3)
k	Consistency factor ($Pa{\cdot}s^n$)
n	Power-law index (1)
τ	Deviator shear stress (Pa)
τ_y	Yield stress (Pa)
U	Velocity domain (m/s)
u_{ini}	Initial velocity (m/s)
p_{in}	Inlet pressure (Pa)

Funding

This research did not receive any external funding.

Data availability statement

The datasets used and/or analyzed during the current study are available from co-author Prof. Abdelaziz Rabehi ($rab\_ehi@hotmail.fr$)on reasonable request.

Declaration of interests

The authors declare that they have no known competing financial interests or personal relationships that could have appeared to influence the work reported in this paper.

Acknowledgements

The researchers wish to extend their sincere gratitude to the Deanship of Scientific Research at the Islamic University of Madinah (KSA) for the support provided to the Post-Publishing Program.

1. R. P. Chhabra, Non-Newtonian fluids: An introduction, In J. Krishnan, A. Deshpande, and P. Kumar, eds., Rheology of Complex Fluids, chap. 1 (Springer, New York, NY, 2010).

2. L. Min, E. Erwin, and H. M. Jennings, Colloid stability of clay suspensions and its role in the formation of kaolinite gels, *Journal of Materials Science* **29** (1994) 1374.

3. R. R. Huilgol and Z. You, Application of the augmented Lagrangian method to steady pipe flows of Bingham, Casson and Herschel-Bulkley fluids, *Journal of Non-Newtonian Fluid Mechanics* **128** (2005) 126.

4. S. K. Vajravelu *et al.*, Mathematical model for a Herschel-Bulkley fluid flow in an elastic tube, *Central European Journal of Physics* **9** (2011) 1357.

5. P. Saramito, Quelques résultats récents en calcul numérique des écoulements de fluides non-newtoniens: viscoélasticité et viscoplasticité (2007).

6. E. Gryparis and G. C. Georgiou, Torsional parallel plate flow of Herschel-Bulkley fluids with wall slip, *Physics of Fluids* **36** (2024) 043122.

7. T. C. Papanastasiou, Flows of materials with yield, *Journal of Rheology* **31** (1987) 385.
8. M. Bercovier and M. Engelman, A finite-element method for incompressible non-Newtonian flows, *Journal of Computational Physics* **36** (1980) 313.
9. R. I. Tanner and J. F. Milthorpe, Numerical simulation of the flow of fluids with yield stress, In C. Taylor, J. A. Johnson, and W. R. Smith, eds., Numerical Methods in Laminar and Turbulent Flow, pp. 680-690 (Pineridge Press, Swansea, UK, 1983).
10. J. D. Dent and T. E. Lang, A Biviscous modified Bingham model of snow avalanche motion, *Annals of Glaciology* **4** (1983).
11. H. Zhu, Y. D. Kim, and D. Dekee, Non-Newtonian fluids with a yield stress, *Journal of Non-Newtonian Fluid Mechanics* **129** (2005) 177.
12. M. A. Hassan, M. Patnak, and M. K. Khan, Rayleigh- Benard Convection in Herschel-Bulkley fluid, *Journal of Non- Newtonian Fluid Mechanics* **226** (2015) 32.
13. S. Mossaz, P. Jay, and A. Magnin, Criteria for the appearance of recirculating and non-stationary regimes behind a cylinder in a viscoplastic fluid, *Journal of Non-Newtonian Fluid Mechanics* **165** (2010) 1525.
14. D. L. Tokpavi, A. Magnin, and P. Jay, Very slow flow of Bingham viscoplastic fluid around a circular cylinder, *Journal of Non-Newtonian Fluid Mechanics* **154** (2008) 65.
15. A. Syrakos, G. C. Georgiou, and A. N. Alexandrou, Thixotropic flow past a cylinder, *Journal of Non-Newtonian Fluid Mechanics* **220** (2015) 44.
16. T. Zisis and E. Mitsoulis, Viscoplastic flow around a cylinder confined in a channel, *Journal of Non-Newtonian Fluid Mechanics* **105** (2002) 1.
17. D. L. Tokpavi, A. Magnin, and P. Jay, Very slow flow of Bingham viscoplastic fluid around a circular cylinder, *Journal of Non-Newtonian Fluid Mechanics* **154** (2008) 65.
18. G. R. Burgos and A. N. Alexandrou, Flow development of Herschel-Bulkley fluids in a sudden three-dimensional square expansion, *Journal of Rheology* **43** (1999) 485.
19. E. Mitsoulis, Numerical simulations of complex yield-stress fluid flows, *Chemical Engineering Science* **59** (2004) 789.
20. E. Mitsoulis, Numerical simulation of calendering viscoplastic fluids, *Journal of Non-Newtonian Fluid Mechanics* **154** (2008) 77.
21. A. A. Gavrilov, K. A. Finnikov, and E. V. Podryabinkin, Modeling of steady Herschel-Bulkley fluid flow over a sphere, *Journal of Engineering Thermophysics* **26** (2017) 197.
22. S. W. Jeong, Determining the viscosity and yield surface of marine sediments using modified Bingham models, *Journal of Geosciences* **17** (2013) 241.
23. S. Patel and R. Chhabra, Steady flow of Bingham plastic fluids past an elliptical cylinder, *Journal of Non-Newtonian Fluid Mechanics* **202** (2013) 32.
24. Y. Lin *et al.*, Concentration dependence of yield stress and dynamic moduli of kaolinite suspensions, *Langmuir* **31** (2015) 4791.
25. S. Mossaz, P. Jay, and A. Magnin, Rheological properties of polymer gels under shear, *Journal of Non-Newtonian Fluid Mechanics* **189-190** (2012) 40.
26. H. Taibi and F. Messelmi, Effect of yield stress on the behavior of rigid zones during the laminar flow of Herschel-Bulkley fluid, *Alexandria Engineering Journal* **57** (2017) 1109.
27. P. Saramito, A new elastoviscoplastic model based on the Herschel-Bulkley viscoplastic model, *Journal of Non- Newtonian Fluid Mechanics* **158** (2009) 154.
28. E. Moreno, A. Larese, and M. Cervera, Modelling of Bingham and Herschel-Bulkley flows with mixed P1/P1 finite elements stabilized with orthogonal subgrid scale, *Journal of Non- Newtonian Fluid Mechanics* **228** (2016) 1.
29. R. B. Spelay, Solids Transport in Laminar, Open Channel Flow of Non-Newtonian Slurries, Ph.D. thesis, University of Saskatchewan, Department of Chemical Engineering, Saskatoon, Saskatchewan (2007).
30. F. Messelmi, Effects of the yield limit on the behavior of Herschel-Bulkley fluid, *Nonlinear Science Letters A* **2** (2011) 137.
31. E. Mitsoulis, Flows of viscoplastic materials: models and computations, *Rheology Reviews* (2007) 135.
32. D. Dent and T. E. Lang, A Biviscous modified Bingham model of snow avalanche motion, *Annals of Glaciology* **4** (1983).
33. H. Zhu, Y. D. Kim, and D. Dekee, Non-Newtonian fluids with a yield stress, *J. Non-Newtonian Fluid Mechanics* **129** (2005) 177.
34. E. Moreno and M. Cervera, Elementos finitos mixtos estabilizados para flujos confinados de Bingham y de Herschel- Bulkley. Parte I: Formulación, *Revista Internacional de Métodos Numéricos para Cálculo y Diseño en Ingeniería* **32** (2016) 100.
35. C. M. Bui and T. X. Ho, Numerical study of an unsteady flow of thixotropic liquids past a Cylinder, *AIP Advances* **9** (2019) 115002.
36. J. Bleyer *et al.*, Efficient numerical computations of yield stress fluid flows using second-order cone programming, *Computer Methods in Applied Mechanics and Engineering* **283** (2015) 599.
37. M. Ali *et al.*, A robust deep learning approach for photovoltaic power forecasting based on feature selection and variational mode decomposition, *Journal of the Nigerian Society of Physical Sciences* (2025) 2795.
38. M. S. Ouahabi *et al.*, Real-Time Sensor Fault Tolerant Control of DC-DC Converters in DC Microgrids Using a Switching Unknown Input Observer, IEEE Access (2023)
39. R. Khelifi *et al.*, Short-Term PV Power Forecasting Using a Hybrid TVF-EMD-ELM Strategy, *International Transactions on Electrical Energy Systems* **2023** (2023) 6413716.
40. A. Rabehi *et al.*, Accurate parameter estimation of Au/GaN/GaAs schottky diode model using grey wolf optimization, *Rev. Mex. Fís.* **70** (2024) 021004.